Energetics and structure of ^{4}He droplets at a finite temperature

C. L. Cleveland, Uzi Landman, and R. N. Barnett
School of Physics, Georgia Institute of Technology, Atlanta, Georgia 30332
(Received 18 August 1988)

Bound quantum-liquid $(^4He)_n$ droplets ($n=57$, 120, and 270) at 3 K coexisting with saturated vapor are studied with use of quantum path-integral molecular dynamics. The diffuse nature of the droplets and their pachydermatous behavior extends to larger sizes in comparison to the corresponding clusters at zero temperature. For the largest droplet a core liquid region develops, exhibiting properties in agreement with bulk data.

I. INTRODUCTION

The stability and structure of rare-gas clusters have been the subject of several recent experimental and theoretical investigations.[1] Among these systems, clusters of helium atoms[2-5] are unique due to their dominant quantum character. Furthermore, these clusters possess several properties which motivate their study. (1) ^{4}He clusters are the only ones that are definitely liquid, since even at 0 K ^{4}He solidifies only at a pressure larger than 25 atm.[6] (2) Their electronic structure is the simplest of all the rare gases which makes them amenable to accurate calculations. (3) Accurate interatomic interaction potentials are available.[7] (4) Quantum-liquid drops can serve as prototype systems for studies of inhomogeneous quantum systems. (5) The similarity between their interaction potentials and the nucleon-nucleon potential[8] (spin-isospin averaged), coupled with their inherent quantum nature, suggests that studies of these clusters will enhance our understanding of the structure, energetics, and dynamics of nuclear matter.

The ground states (at zero temperature) of ^{4}He and ^{3}He clusters have been studied recently using the Green's-function Monte Carlo (GFMC),[9] variational Monte Carlo (VMC),[10] and density-functional (DF)[11,12] methods. We present results of quantum path-integral molecular-dynamics (QUPID) simulations[13] of liquid $(^4He)_n$ droplets ($n=57$, 120, and 270) which provide information about the effect of finite temperature (3 K) on the energetics and structure of these clusters in equilibrium under saturated-vapor-pressure (SVP) conditions.

II. METHOD

The method which we used rests on the Feynman path-integral formulation of statistical mechanics,[14] which allows the derivation of an expression for the partition function Z, for a system of N quantum particles (mass m), $Z=\lim_{P\to\infty} Z_P$, which neglecting exchange, can be written as

$$Z_P=\left[\frac{mP}{2\pi\hbar^2\beta}\right]^{3NP/2}\int\prod_{i=1}^{N}\prod_{p=1}^{P}d\mathbf{r}_{ip}\,e^{-\beta V_{\rm eff}}\,, \tag{1a}$$

$$V_{\rm eff}=\frac{Pm}{2\hbar^2\beta^2}\sum_{i=1}^{N}\sum_{p=1}^{P}(\mathbf{r}_{ip}-\mathbf{r}_{ip+1})^2+\frac{1}{P}\sum_{1\le j<i\le N}\sum_{p=1}^{P}V(\mathbf{r}_{ip}-\mathbf{r}_{jp})\,, \tag{1b}$$

where V is the interparticle interaction potential and $\beta=1/k_BT$. Equation (1) establishes an isomorphism between the quantum problem and a classical one where each quantum particle is represented by a harmonic cyclic chain ($\mathbf{r}_{i,P+1}\equiv\mathbf{r}_{i1}$) of P pseudoparticles.[13] The equilibrium average energy of the system is given by

$$E=\frac{3N}{2\beta}+K_{\rm int}+\langle U\rangle\,, \tag{2a}$$

where U is the second term in Eq. (1b), the angular brackets denote averages over the statistical distribution defined by Eq. (1), and the interaction kinetic energy is given by[13b,15]

$$K_{\rm int}=\frac{1}{2P}\sum_{i=1}^{N}\sum_{p=1}^{P}\left\langle\frac{\partial V}{\partial\mathbf{r}_{ip}}\cdot(\mathbf{r}_{ip}-\mathbf{r}_{iP})\right\rangle\,. \tag{2b}$$

Thus the kinetic energy $\langle K\rangle$ is given by the sum of the first two terms in Eq. (2a).

The equilibrium averages may be obtained via classical molecular dynamics[15] (MD) by noting the equivalence between the canonical statistical averages defined by Eq. (1) and averaging, using constant temperature MD,[16] over the classical phase-space trajectories generated by a Hamiltonian with $V_{\rm eff}$ [Eq. 1(b)] as the potential term augmented with a kinetic energy of the pseudoparticles. The number of pseudoparticles P which is required to achieve convergence is temperature dependent. In our calculations, at 3 K, $P=64$ yields convergent results. The interparticle potential which we used is the HFDHE2 potential of Aziz *et al.*[7] and the equations of motion were integrated using the velocity form of the Verlet algorithm, with a time step $\Delta t=2.06\times10^{-15}$ sec.

III. RESULTS

Since at finite temperatures and zero pressure the equilibrium state of helium is a gas,[6] in order to investigate a condensed state we confine the system in a spherical cavity[17] of radius R_c (defined as the distance from the center

at which the repulsive confining potential vanishes). Consequently, an equilibrium coexistence between a condensed phase and a surrounding vapor can be established. At the temperature of our study (3 K) effects due to exchange on structural and energetic properties of liquid ^{4}He are very small.[14,18–20] However, the quantum nature of the system is manifest. In fact pure classical simulations yield a solid under these conditions. Moreover, simulations using the Feynman-Hibbs smoothed effective potential[14] yield unstable clusters (since the width of the Gaussian-smearing function used in this method corresponds to the thermal wavelength of a *free particle,* while particles in the quantum liquid are more localized, see below).

Three systems were studied: I, $N=70$, $R_c=34.6a_0$; II, $N=150$, $R_c=44.6a_0$; and III, $N=294$, $R_c=44.6a_0$. Prolonged equilibration and averaging periods [typically $(2-4)\times10^5\Delta t$] were necessary since the process of exploration of the accessible phase space in these systems is rather slow. For the large system (III), simulations on an ETA-10G computer, using a fully optimized code required 1.75 CPU h per $10^3\Delta t$. In Fig. 1 we exhibit plots versus distance from the center of the cavity of the number density, $\rho(r), n(r)=\int_0^r \rho(\mathbf{r}')d\mathbf{r}'$, the per-particle total energy E and its potential and interaction-kinetic-energy components, $\langle U\rangle$ and $\langle K_{\rm int}\rangle$, respectively, and of the rms radius of the ^{4}He atoms,

$$R_g^2=\frac{1}{2P^2}\left\langle \sum_{p,p'=1}^{P}(\mathbf{r}_p-\mathbf{r}_{p'})^2\right\rangle . \tag{3}$$

In constructing the radial plots the desired property is averaged over the trajectories of atoms whose pseudoparticles' barycenters lie in spherical shells $(r,r+\Delta r)$ of equal volumes.

The values of characteristic quantities obtained in this as well as other studies are given in Table I. These quantities include the average energy per particle, E; the central density ρ_c, calculated for the central region of the cluster, i.e., for atoms whose barycenters are within a distance $\bar{r}$ from the center where $\bar{r}=10a_0$ for system I and $12.5a_0$ for systems II and III; the relative compression $\delta\rho/\rho_0=(\rho_c-\rho_0)/\rho_0$, where ρ_0 is the experimental bulk density at the corresponding temperature on the vaporization curve; the width of the interface of the liquid cluster t, defined as the distance between the radii where the density $\rho(\mathbf{r})$ has decreased from the central value ρ_c by 90% and 10% of the difference between ρ_c and the density ρ_v in the surrounding vapor (see below); the unit radius $r_0=(\frac{5}{3}\langle r^2\rangle)^{1/2}N^{-1/3}$, where $\langle r^2\rangle=\int d\mathbf{r}\,\rho(r)r^2/N$, and $r_{1/2}$ defined as the distance for which $\rho(r_{1/2})=(\rho_c-\rho_v)/2$.

As seen from Fig. 1(a) the density of the clusters decreases monotonically from the center outwards culminating in a shell of constant density corresponding to the coexisting vapor. Thus for a given radius of the cavity and number of particles N the system achieves an equilibrium coexistence between a critical liquid droplet and its saturated vapor.[21] The spatial extent of the liquid droplet is the distance R_l at which the transition to vapor occurs which is determined to be, for the I-III systems, $28a_0$ ($n=57$), $35a_0$ ($n=120$), and $39a_0$ ($n=270$), respectively, where n is the number of atoms comprising the liquid droplet [see Fig. 1(b)]. The liquid-droplet quantities in Table I are calculated for these $(^4\mathrm{He})_n$ clusters, i.e., excluding the vapor. As evident, the central density increases with cluster size (see Table I) and for

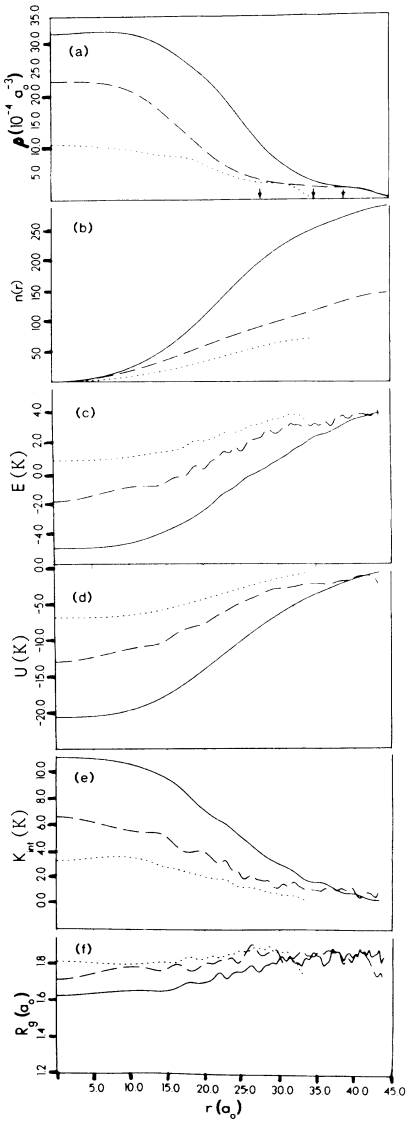

FIG. 1. Results obtained via QUPID calculations at 3 K for equilibrium liquid ^{4}He clusters at SVP conditions. The solid, dashed, and dotted lines correspond to system sizes N of 70 (57), 150 (120), and 294 (270) atoms, respectively (the numbers of particles in parenthesis correspond to the sizes of the liquid droplets in coexistence with a surrounding vapor). Plots vs distance (in Bohr radii) from the center of the droplets are shown for (a) the number density $\rho(r)$. The arrows indicate the radii of the liquid droplets ($28a_0$, $35a_0$, and $39a_0$). The vanishing of the density for $r\to R_c$ is due to the confining potential; (b) the number of atoms $n(r)$; (c)–(e) the per-particle total energy E and its potential U and interaction kinetic energy $K_{\rm int}$ components; (f) the rms spatial spread R_g of the atoms.

the smaller clusters (I and II) is significantly lower than that obtained in the 0 K calculations.[10,11] For the larger clusters (III) ρ_c is in agreement with those calculations[10,11] and is close to the experimental bulk value[22] at 3 K along the vaporization curve ($3.14\times10^{-3}a_0^{-3}$), as are also the SVP vapor density (ρ_v) and pressure (P_v). Experimentally[22] at 3 K $\rho_v=9.55\times10^{-5}a_0^{-3}$ and $P_v=0.25$ atm. The calculated values for systems I-III are $\rho_v=3.17\times10^{-4}a_0^{-3}$, $2.21\times10^{-4}a_0^{-3}$, $2\times10^{-4}a_0^{-3}$, and $P_v=0.52$, 0.45, and 0.35 atm, respectively. We should caution that for all our systems corrections due to finite size (surface energy and curvature) are significant and thus the comparisons to experimental thermodynamic data should be regarded as qualitative and suggestive (in particular for interfacial quantities which are most sensitive to these effects).

While the three different size droplets are found to be bound in our calculations at 3 K (indeed studies at 0 K predict[9-11] that ^{4}He clusters are always bound and that the Bose nature does not suggest any kind of magic-number stabilities due to filling of single particle levels, unlike the case of ^{3}He clusters[10-12]), the nature and structure of the droplets vary significantly depending on their size and on temperature. This can be seen best by examining the calculated relative compressions $\delta\rho/\rho_0$ for the three clusters (Table I). We observe that the ^{4}He droplets exhibit a pachydermatous behavior (i.e., less compressed than the bulk material) even at relatively large sizes [$\delta\rho/\rho_0<0$ for I ($n=57$) and II ($n=120$) in Table I], and comparison to the 0 K calculations reveals that the magnitude of the effect is larger at finite temperature and extends to larger clusters (at 0 K $\delta\rho/\rho_0>0$ already for $n=64$, see Fig. 3, in Ref. 11). This indicates that the effect of temperature is to increase the size range for which the diffuseness of the clusters (i.e., the lack of clear distinction between surface and volume regions) dominates the compressive contribution due to the surface energy,[11] resulting in an increase of the critical cluster size for which the transition from pachydermatous to leptodermous ($\delta\rho/\rho_0>0$) behavior occurs. In addition we note (see Table I) that the calculated unit radii r_0 which is a measure of the average volume per atom in the cluster, are larger at finite temperature in comparison to the 0 K results[10,11] and the experimental value[21] for bulk liquid ^{4}He at 3 K ($r_0=4.236a_0$).

To analyze the energetics of the clusters we exhibit in Fig. 1(c)–1(e) radial plots of the total energy per atom E and of the potential and interaction-kinetic-energy contributions $\langle U\rangle$ and $\langle K_{\rm int}\rangle$, respectively [see Eq. (2)]. It is seen that the binding energies decrease going outwards from the center of the droplets. Consistent with our previous discussion, we observe that only for the largest cluster [(^{4}He)$_{270}$, solid line in Fig. 1] the binding energy at the central (core) region is close (-4.945 K) to the bulk liquid value at 3 K (-4.78 K from experiment[22] and -4.92 K from path-integral Monte Carlo[18]). In addition we note that the energy per particle in the vapor region for all three clusters is close to the experimentally estimated value[22] (3.97 K).

The variations of the potential and kinetic energy con-

TABLE I. Results of our path-integral (QUPID) calculations at 3 K for equilibrium liquid (^{4}He)$_n$ ($n=57$, 120, and 270) droplets at SVP conditions, as well as those obtained for these size clusters at 0 K via the DF (Ref. 11) and VMC (Ref. 10) methods. For the per-particle energy E obtained in our calculations, both values averaged over the entire droplet, and those corresponding to particles in the core region ($10a_0$ for I and $12.5a_0$ for II and III) are given. In the bottom two rows experimental (Ref. 22) and calculated results for bulk and free surface liquid ^{4}He, at 0 and 3 K are given. Energy in degrees Kelvin and distances in Bohr radii. For the energies and r_0 statistical uncertainties are defined as $(\langle x^2\rangle-\langle x\rangle^2)^{1/2}/N_r^{1/2}$, where the quantity in question x is averaged over N_r simulation steps separated by $50\Delta t$, $N_r=5840$, 2200, and 2160 for systems I, II, and III, respectively.

	E (K)			$\rho_c(10^{-3}a_0^{-3})$			$\delta\rho/\rho_0$			$t(a_0)$			$r_0(a_0)$			$r_{1/2}(a_0)$		
(^{4}He)$_n$	57	120	270	57	120	270	57	120	270	57	120	270	57	120	270	57	120	270
QUPID (3 K)	2.054	0.850	−1.285	1.07	2.35	3.19	−0.66	−0.25	0.016	15.9	15.9	17.0	6.755	6.033	4.872	20	17	24
	±0.012	±0.017	±0.014										±0.005	±0.002	±0.001			
(CORE)	(0.828)	(−1.862)	(−4.945)															
	±0.057	±0.070	±0.068															
DF[a]	−2.605	−3.574	−4.407	3.19	3.38	3.41	−0.018	0.042	0.051	17.2	17.6	17.6	4.50	4.65	4.44	15	19	26
VMC[b]	−2.753	−3.541	−4.239	3.07	3.37	3.33	−0.050	0.043	0.031		∼13		4.74	4.59	4.47			
Bulk (3 K)	−4.78 (expt[c]); −4.92 (QMC[d])			3.14 (expt[c])			0			free surface (DF[e])			4.236 (expt[c])			free surface (DF[e])		
Liquid (0 K)	−7.17 (expt[c])			3.23 (expt[c])			0			13.4 (at 0 K)			4.196 (expt[c])			19 (at 0 K)		

[a] Reference 11. [d] Reference 18.
[b] Reference 10. [e] Reference 23.
[c] Reference 22.

tributions with distance from the center of the droplet reflect the variations in density [Fig. 1(a)] and degree of particle quantum localization [see radial R_g results in Fig. 1(f)]. For an equilibrium system of noninteracting quantum ^{4}He particles at 3 K the energy per particle is $K_f = 4.5$ K (i.e., $3k_BT/2$) and the rms spread of each particle $[R_g^f = \hbar(3\beta/8m)^{1/2}]$ is $2.33a_0$. The interatomic interactions serve to decrease the quantum spatial spread of the ^{4}He atoms (i.e., $R_g < R_g^f$). The degree of quantum localization, which increases with cluster size, is evident from Fig. 1(f). Furthermore, the degree of localization is largest in the core regions of the droplets, decreasing as a function of distance from the center (most pronounced for the largest cluster, solid line). Note however that even particles in the vapor region exhibit a significant degree of quantum localization. The interactions make also a contribution to $K_{\rm int}$ [Fig. 1(e)] which combined with K_f and the potential energy [Fig. 1(d)] yield the total energy E [Fig. 1(c)]. We remark that for the smallest cluster [$(^4\text{He})_{57}$, dotted line] the kinetic energy is larger than the potential contribution resulting in a positive value for E throughout the droplet.

Pair distribution functions for the three clusters are shown in Fig. 2. In the Appendix, we define a pair distribution function for clusters $g(r_1,r_2,r_{12})$, where r_1 and r_2 are the radial distances from the center of the cluster of two particles and r_{12} is their interparticle separation. The method of calculating $g(r_1,r_2,r_{12})$ which we use is also described in the Appendix.

Once the $g(r_1,r_2,r_{12})$ have been so calculated, they may be averaged together in various ways to improve statistics and make them more readily presentable. As pointed out by Pieper *et al.*,[24] if we consider $g(r_1,r_2,r_{12})$ to be a function of r_{12}, taking r_1 and r_2 as parameters, the function depends on $R_m = |r_1 + r_2|/2$ much more strongly than on $|r_1 - r_2|$, so that we may average all the $g(r_1,r_2,r_{12})$ for which R_m lies within some specified range and consider the result $g(R_m,r_{12})$ to be a function of R_m and r_{12}. It is these $g(R_m,r_{12})$ which are shown in Fig. 2.

The results for $g(R_m,r_{12})$ in Fig. 2 are given for $R_m \le 15a_0$ for system I (dotted) and $R_m \le 10a_0$ for systems II and III (dashed and solid lines, respectively). We note that while the heights of the first peaks are similar for the three systems, the peak broadens and its maximum shifts to larger values of r_{12} with decrease in the number of particles in the droplet, consistent with the variation in density in the central regions of these systems [see Fig. 1(a) and Table I]. Furthermore, upon increasing the size of the droplet the second coordination shell develops.

In Fig. 3 we reproduce the experimentally measured bulk[25] pair distribution function, at 3 K (dashed line), as well as the calculated $g(R_m,r_{12})$ functions for the largest droplet ($n = 270$) for $R_m \le 10a_0$ (solid line) and for $20a_0 \le R_m \le 25a_0$ (dotted line). In comparing the calculated and experimental results we note that the $g(R_m,r_{12})$ function for the central region of the droplet exhibits similar features to the experimental curve. This agreement indicates that the core region of the large droplet develops bulklike characteristics. The deviations from the bulk properties are enhanced in the pair distribution function corresponding to a lower density region of the droplet (dotted line). In fact a comparison of this $g(R_m,r_{12})$ function with the one for the core region of the medium size droplet ($n = 120$) shown in Fig. 2 (dashed line), i.e., for two regions of comparable density in two different systems, shows that they are extremely similar, supporting the suggestion[24] that these pair distribution functions are largely governed by the density at R_m.

The first minima in the $g(R_m,r_{12})$ in Fig. 2 occur at $11.55a_0$, $10.65a_0$, and $9.90a_0$ for systems I, II, and III, in

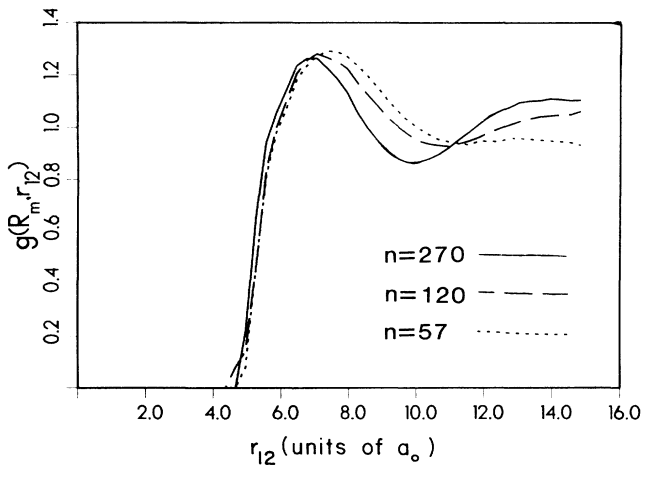

FIG. 2. Results for the pair distribution function $g(R_m,r_{12})$ for the three $(^4\text{He})_n$ droplets at 3 K: $n = 57$ ($R_m \le 15a_0$, dotted), $n = 120$ ($R_m \le 10a_0$, dashed), and $n = 270$ ($R_m \le 10a_0$, solid). Note the broadening and shift of the first peak to larger values of r_{12} with decrease in the droplet size, and the development of the second coordination shell for the larger droplets.

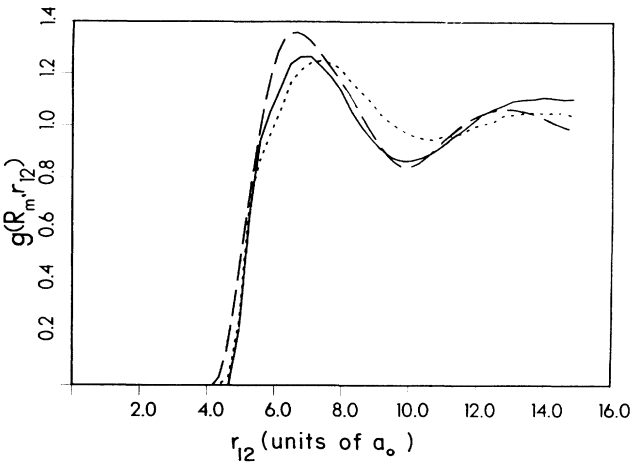

FIG. 3. Calculated pair distribution functions $g(R_m,r_{12})$ for the $(^4\text{He})_{270}$ droplet at 3 K for two values of R_m; $R_m \le 10a_0$ (solid) and $20a_0 \le R_m \le 25a_0$ (dotted). The experimental bulk pair distribution function measured (Ref. 25) at 3 K is given for comparison (dashed line).

order of increasing system size. For the experimental bulk curve it occurs at $9.88a_0$. If we take all the atoms closer than the first minimum to be nearest neighbors, then the experimental bulk system has 11.96 nearest neighbors. If we count the number of barycenters within the first minimum in the $g(R_m, r_{12})$ from our simulations, we find 6.83, 11.62, and 11.61 for systems I, II, and III, respectively. Note that although the nearest-neighbor shell for the medium-size droplet (system II) is more diffuse than that of the large droplet (system III), the number of nearest neighbors in these two shells is essentially the same, and near the experimental result for bulk He at the same temperature.

IV. SUMMARY

From these studies we conclude that bound quantum-liquid $(^4\text{He})_n$ droplets can form at finite temperature (3 K) under SVP conditions, thus extending the predictions of 0 K calculations[9–12] to the finite-temperature domain. Our results reveal significant temperature effects on the energetics and structure of the clusters. Although characteristics of the radial-density profiles (surface width, t, and r_{12}, see Table I) in our calculations are comparable to the values obtained in previous studies,[10,11] we find that ^{4}He droplets at 3 K are more diffuse and less bound in comparison to the corresponding clusters at zero temperature (see per-particle energies, ρ_c and r_0 in Table I for $n=57$ and 120). Thus, at 3 K, even in the core region of the droplets bulk values are approached only for rather large clusters, and the pachydermatous behavior (core density deficiency compared to bulk) extends to large clusters. Finally, we note that the systems which we studied are of a pronounced quantum character, which varies across the system [see the quantum spread R_g in Fig. 1(f)], thus suggesting them as prototype systems for investigations of inhomogeneous quantum matter.

ACKNOWLEDGMENTS

This research was supported by the U.S. Department of Energy Grant No. FG-05-86ER45234. Most of the calculations were performed on the ETA-10G computer at the Florida State University Supercomputer Computation Research Institute (Tallahassee, FL), made possible by a grant of computer time by the U.S. Department of Energy.

APPENDIX

We begin with the usual definition of a pair distribution function in an inhomogeneous system,

$$\tilde{g}_2(\mathbf{s}_1,\mathbf{s}_2)=\rho_2(\mathbf{s}_1,\mathbf{s}_2)/[\rho(\mathbf{s}_1)\rho(\mathbf{s}_2)] , \tag{A1}$$

where $\rho(\mathbf{s})$ and $\rho(\mathbf{s}_1,\mathbf{s}_2)$ are the one- and two-particle densities, respectively. Unfortunately, this function depends on too many coordinates to be conveniently displayed. We can exploit the spherical symmetry of our clusters to reduce somewhat the number of variables. The strategy is to average the pair distribution function of Eq. (A1) over values of $\mathbf{s}_1$ and $\mathbf{s}_2$ such that (1) $\mathbf{s}_1$ falls in a spherical shell of mean radius r_1 and width Δ_1, (2) $\mathbf{s}_2$ falls in a spherical shell of mean radius r_2 and width Δ_2, and (3) the distance between the two particles $s_{12}=|\mathbf{s}_2-\mathbf{s}_1|$ falls between $r_{12}-\Delta_{12}/2$ and $r_{12}+\Delta_{12}/2$, for a chosen width Δ_{12}. If we now define a function $P(\mathbf{s}_1,\mathbf{s}_2;r_1,r_2,r_{12})$ to be equal to one if these conditions are satisfied and zero otherwise, we can write

$$\tilde{g}(r_1,r_2,r_{12})=v_2^{-1}\int d^3s_1\int d^3s_2\, P(\mathbf{s}_1,\mathbf{s}_2;r_1,r_2,r_{12})\tilde{g}_2(\mathbf{s}_1,\mathbf{s}_2) , \tag{A2}$$

where

$$v_2=\int d^3s_1\int d^3s_2\, P(\mathbf{s}_1,\mathbf{s}_2;r_1,r_2,r_{12}) . \tag{A3}$$

The spherical symmetry of the system allows us to take $\rho(\mathbf{s})=\rho(s)$, so that using Eq. (A1) we may rewrite Eq. (A2) as

$$\tilde{g}(r_1,r_2,r_{12})=[v_2\rho(r_1)\rho(r_2)]^{-1}\int d^3s_1\int d^3s_2\, P(\mathbf{s}_1,\mathbf{s}_2;r_1,r_2,r_{12})\rho_2(\mathbf{s}_1,\mathbf{s}_2) \tag{A4}$$

if Δ_1 and Δ_2 are small enough so that ρ does not vary significantly across the radial bins. The integrals in Eq. (A4) may be evaluated simply by counting how many pairs of atoms are found in the system satisfying the conditions which make P equal to one, and of course $\rho(r)$ may be simultaneously accumulated. The only remaining difficulty is to evaluate v_2. While this task is quite arduous for arbitrary choices of the Δ's, if they are small it is easy to show that v_2 may be accurately approximated by

$$v_2=8\pi^2 r_1 r_2 r_{12}\Delta_1\Delta_2\Delta_{12} . \tag{A5}$$

Using Eq. (A5) allows us to finish the evaluation of $\tilde{g}(r_1,r_2,r_{12})$.

In performing these calculations for our system, the "particles" gone over should be the pseudoparticles onto which the atoms are mapped in the "classical isomorphism,"[13,14] since the pseudoparticle density anywhere is the probability per unit volume of finding an atom there, with the understanding that two pseudoparticles corresponding to the same atom do not contribute to the pair distribution function. However, because of their volume, records of all the pseudoparticle positions were not recorded for all the computer runs used for averaging; only properties of atoms as a whole, such as the location of each atom's barycenter (center of number of the corresponding pseudoparticles) and radius of gyration of the pseudoparticle distributions, were always recorded. Thus in calculating the pair distribution

function an approximate account of the distribution of pseudoparticles about each atom's barycenter is necessary.

We now describe our approach to this problem. First we calculate $\tilde{g}(r_1,r_2,r_{12})$ for the barycenters. For each value of r_1 and r_2 we have in this pair distribution function a function of the magnitude r_{12} alone; for compactness of notation we shall abbreviate and denote it by $\tilde{g}(r_{12})$. This also emphasizes that $\tilde{g}(r_1,r_2,r_{12})$ is a much stronger function of r_{12} than of r_1 or r_2. However, a barycenter at, say, $\mathbf{r}_1$ actually represents a distribution of pseudoparticles around that location. As a correction, we would like to average over this distribution. Because of the nature of the recorded information available to us from our simulation, we take the distribution to be a Gaussian whose standard deviation is chosen to retrieve the average radius of gyration of the pseudoparticle distribution corresponding to an atom whose barycenter is located a distance r from the center of the cluster [see Fig. 1(f)]. That is, we calculate a smoothed $g(r_{12})$ where

$$g(r_{12})=(2\pi\sigma_1\sigma_2)^{-3}\int d^3s_1\int d^3s_2\,\tilde{g}(s_{12})\exp(-|\mathbf{s}_1-\mathbf{r}_1|^2/2\sigma_1^2)\exp(-|\mathbf{s}_2-\mathbf{r}_2|^2/2\sigma_2^2)\ , \tag{A6}$$

where σ_1 is the standard deviation a distance r_1 from the center, and similarly for σ_2. In evaluating Eq. (A6), we adopt the approximation, $\tilde{g}(s_{12})\equiv\tilde{g}(s_1,s_2,s_{12})\cong\tilde{g}(r_1,r_2,s_{12})$.

With $\sigma^2=\sigma_1^2+\sigma_2^2$, it is easy to show from Eq. (A6) that if r_{12} is nonzero,

$$g(r_{12})=(\sqrt{2\pi}\sigma r_{12})^{-1}\int ds_{12}\,\{\exp[-(s_{12}-r_{12})^2/2\sigma^2]-\exp[-(s_{12}+r_{12})^2/2\sigma^2]\}s_{12}\tilde{g}(s_{12})\ , \tag{A7}$$

while if r_{12} is zero,

$$g(0)=2(\sqrt{2\pi}\sigma^3)^{-1}\int ds_{12}\exp(-s_{12}^2/2\sigma^2)s_{12}^2\tilde{g}(s_{12})\ . \tag{A8}$$

Of course, this approach ignores correlations in the distributions of pseudoparticles about two neighboring barycenters. The neglect of such correlations appears to be relatively unimportant, however, unless the two atoms are so close (closer than about $5a_0$) that the hard-core repulsion between them comes into play, causing the distributions to become markedly asymmetric. Consequently, for interparticle distances closer than about $5a_0$, a $g(r_{12})$ smoothed by this prescription goes to zero much too slowly as r_{12} goes to zero. We have tried to roughly compensate for this defect by imposing on the smoothing in Eqs. (A7) and (A8) the constraint that $g(r_{12})$ be zero if $g(r_{12})$ is, although this causes $g(r_{12})$ to go to zero somewhat too rapidly as r_{12} goes to zero. In any case, the effect of this compensation is negligible if r_{12} exceeds $5a_0$, and values for r_{12} less than $5a_0$ should not be taken as quantitatively accurate.

[1]See the following reviews and references therein: R. S. Berry, T. L. Beck, and H. L. Davis, in *Physics and Chemistry of Small Clusters,* edited by P. Jena, B. K. Rao, and S. N. Khanna (Plenum, New York, 1986), p. 185; J. Farges, M. F. de Feraudy, B. Raoult, and G. Torchet, *ibid.,* p. 15; M. R. Hoare, Adv. Chem. Phys. **40**, 49 (1979); N. Schwenter, E. E. Koch, and J. Jortner, *Electronic Excitations in Condensed Rare Gases* (Springer, Berlin, 1985); U. Landman, R. N. Barnett, J. Luo, D. Scharf, and J. Jortner, in *Few-Body Systems and Multiparticle Dynamics, (Crystal City, VA, 1987),* Proceedings of the Conference on Few-Body Systems and Multiparticle Dynamics, AIP Conf. Proc. No. 162, edited by D. A. Micha (AIP, NY, 1987), p. 200.

[2]E. W. Becker, K. Bier, and W. Henkes, Z. Phys. **146**, 333 (1956); J. Gspann, Physica (Utrecht) **108B**, 1309 (1981).

[3]A. P. J. van Deursen and J. Reuss, J. Chem. Phys. **63**, 4559 (1975).

[4]P. W. Stephens and J. G. King, Phys. Rev. Lett. **51**, 1538 (1983).

[5]H. Buchenau, R. Gotting, A. Scheidemann, and J. P. Toennies, in *Flow of Real Fluids,* edited by G. E. A. Meier and F. Obermeier (Springer, Berlin, 1985), p. 157.

[6]H. R. Glyde, in *Rare Gas Solids,* edited by M. L. Klein and J. A. Venables (Academic, New York, 1976), p. 382.

[7]R. A. Aziz, V. P. S. Nain, J. S. Carley, W. L. Taylor, and G. T. McConville, J. Chem. Phys. **70**, 4330 (1979).

[8]J. H. Rose, J. P. Vary, and J. R. Smith, Phys. Rev. Lett. **53**, 344 (1984).

[9]V. R. Pandharipande, J. G. Zabolitzky, S. C. Perper, R. B. Wiringa, and U. Helmbrecht, Phys. Rev. Lett. **50**, 1676 (1983), and references to earlier work cited therein.

[10]V. R. Pandharipande, S. C. Pieper, and R. B. Wiringa, Phys. Rev. B **34**, 4571 (1986).

[11]S. Stringari and J. Treiner, J. Chem. Phys. **87**, 5021 (1987).

[12]S. Stringari, Phys. Lett. **107A**, 36 (1985).

[13](a) D. Chandler and P. G. Wolynes, J. Chem. Phys. **74**, 4078 (1981); (b) see review by B. J. Berne and D. Thirumalai, Annu. Rev. Phys. Chem. **37**, 401 (1986).

[14]R. P. Feynman and A. R. Hibbs, *Quantum Mechanics and Path Integrals* (McGraw-Hill, New York, 1965); R. P. Feynman, *Statistical Mechanics* (Benjamin, Reading, 1972).

[15]M. Parrinello and A. Rahman, J. Chem. Phys. **80**, 860 (1984).

[16]J. R. Fox and H. C. Anderson, J. Phys. Chem. **88**, 4019 (1984).

[17]For studies of classical Argon clusters employing a constraining volume, see J. K. Lee, J. A. Barker, and F. F. Abraham, J. Chem. Phys. **58**, 3166 (1973).

[18]For studies of liquid ^{4}He employing a Monte Carlo path-integral method and the Aziz potential (Ref. 7), see D. M. Ceperley and E. L. Pollock, Phys. Rev. Lett. **56**, 351 (1986).

[19]In this context we mention studies of helium absorption on graphite, F. F. Abraham and J. Q. Broughton, Phys. Rev. Lett. **59**, 64 (1987).

[20]D. M. Ceperley (private communication).

[21]In this context we remark that there are no solutions of the bulk hypernetted-chain–Euler-Lagrange equations below about 60% of the calculated saturation density, which reflects

the instability of a low-density fluid against droplet formation; see L. Castillejo, A. D. Jackson, B. K. Jennigs, and R. A. Smith, Phys. Rev. B **20**, 3631 (1979).

[22]R. K. Crawford, in *Rare Gas Solids,* edited by M. L. Klein and J. A. Venables, (Academic, New York, 1976), Vol. II, p. 675.

[23]S. Stringari and J. Treiner, Phys. Rev. B **36**, 8369 (1987); for other studies of the free helium surface see K. S. Liu, M. H. Kalos, and G. V. Chester, Phys. Rev. B **12**, 1715 (1975); E. Krotschek, G. X. Qian, and W. Kohn, *ibid.* **31**, 4245 (1985); J. L. Valles and K. E. Schmidt, *ibid.* **38**, 2879 (1988).

[24]S. C. Pieper, R. B. Wiringa, and V. R. Pandharipande, Phys. Rev. B **32**, 3341 (1985).

[25]H. N. Robkoff and R. B. Hallock, Phys. Rev. B **24**, 159 (1981).